Spatiotemporally tuned colloidal phoretic leap in an altering multivalent interaction field

Ekta Shandilya,[a] Bhargav Rallabandi*[b] and Subhabrata Maiti*[a]

[a] Department of Chemical Sciences, Indian Institute of Science Education and Research (IISER) Mohali, Knowledge City, Manauli - 140306, India.

[b] Department of Mechanical Engineering, University of California, Riverside, California - 92521, USA.

*Corresponding author

Email: smaiti@iisermohali.ac.in; bhargav@engr.ucr.edu

Abstract

Multivalency-mediated interactions play an important role in governing dynamicity and self-assembly in biological systems. Despite its significance in supramolecular material chemistry to biomedicine, the role of multivalency in modulating colloidal transport or phoresis remains largely unexplored. Here, combining theory and experiment, we report diffusiophoretic motion of a positively-charged catalytic microbead during its multivalent interactions with a gradient of adenosine mono-, di- and trinucleotides (AM/D/TP) both in micro- and macroscale regimes. We find that the extent of drift diminishes with increasing number of phosphates. Subsequently, we exhibit nucleotide-specificity of the colloid in catalyzing a proton-transfer reaction, which in turn alters its phoretic behaviour. Finally, we demonstrate spatiotemporal control over colloidal phoretic leap (a sudden increase in phoretic velocity) and population dynamics driven by enzymatic downregulation of multivalent interactivity, which we achieve by controlling ATP hydrolysis in situ. These findings open up avenues for utilizing multivalent surface-mediated catalytic activity to achieve precise control of particle transport relevant to reaction-diffusion driven spatiotemporal processes.

Keywords: *Multivalency • Nucleotide • Diffusiophoresis • Colloid • Proton transfer • Enzyme*

Introduction

Multivalent interactions are fundamental in governing both biological and synthetic supramolecular processes.[1-3] In the last two decades, considerable pioneering work has elucidated the role of weak and cooperative binding for strong and specific binding affinity between two entities, involving surfaces.[4-7] Chemists exploit multivalent effects in sensing, catalysis, and designing drug molecules to inhibit viral infection or to achieve desired cellular response by altering biochemical pathways.[8-10] Such interactions among peptides or proteins, carbohydrates, (oligo)nucleotides, or self-assembled monolayer (SAM) containing surface or nanoparticle have been used for both applications and theoretical understanding of the binding and associated functions such as assembly, sensing and catalysis.[11-19] Past work has demonstrated time-regulated dynamic self-assembled systems with simultaneous temporal control over associated functions by modulating non-covalent interactivity between multivalent chemical stimuli and building blocks.[20-25] Nonetheless, the consequences of spatially and temporally varying multivalent interactivity in controlling the motion and thereby spatial distribution and related functions of the interacting species remains underexplored. In a recent study, Wilson et al. reported the diffusiophoretic motion of an anionic microbead in response to a gradient of divalent cation or anion.[26] However, how multivalent interactions and their 'in situ' modulation govern the diffusiophoresis (directional migration of a (bio)colloidal species by sensing concentration gradient of salts in its surroundings) of surface-interactive colloids both in space and time has not been explored.[26-27] Here, we investigate the role of multivalent interactions and their spatiotemporal control for the control of diffusiophoresis, in particular using biologically essential molecules.

Since 1947, after the notable work of Derjaguin followed by Anderson et al., the physicochemical origin of diffusiophoretic transport of colloids in gradient of salts has been established.[28-35] Past studies have been limited to common inorganic salts like NaCl, KCl, $MgCl_2$, etc., featuring mainly halides, nitrates, sulfates, carbonates of group-I and II metal ions of the periodic table.[24-40] In this work, we investigate multivalent interaction-mediated phoretic drift of a fluorescent, cationic micron-sized bead (abbreviated CMB) exposed to gradients of nucleotides, namely adenosine mono/di/triphosphate (AMP/ADP/ATP) and their mixtures in different proportions. The CMB consists of a carboxylic acid-modified polystyrene fluorescent bead electrostatically bound with a cationic cetyltrimethylammonium bromide (CTAB)-coated gold

nanorods (GNR) (Figure 1a).[41] Notably, in cellular systems, diffusiophoretic transport of large molecules due to gradients of small molecules such as metabolites or ATP is ubiquitous, and has recently gained attention.[42-43] Furthermore, analogous to the allosteric activity modulation of enzyme, binding of the nucleotides AMP or ATP can activate or deactivate the proton transfer ability of the CMB.[44-46] We exploit this nucleotide-selective catalytic activation behavior and its effect in modulating the overall phoretic drift of the CMB under both catalytic and non-catalytic conditions. Finally, by exploiting the aforementioned facts we developed an autonomous system where we demonstrate the occurrence of a colloidal phoretic leap (a sudden increase in phoretic velocity) and show how the positioning of the particles can be spatiotemporally programmed, simply using enzymatic in situ downregulation of multivalent interaction.

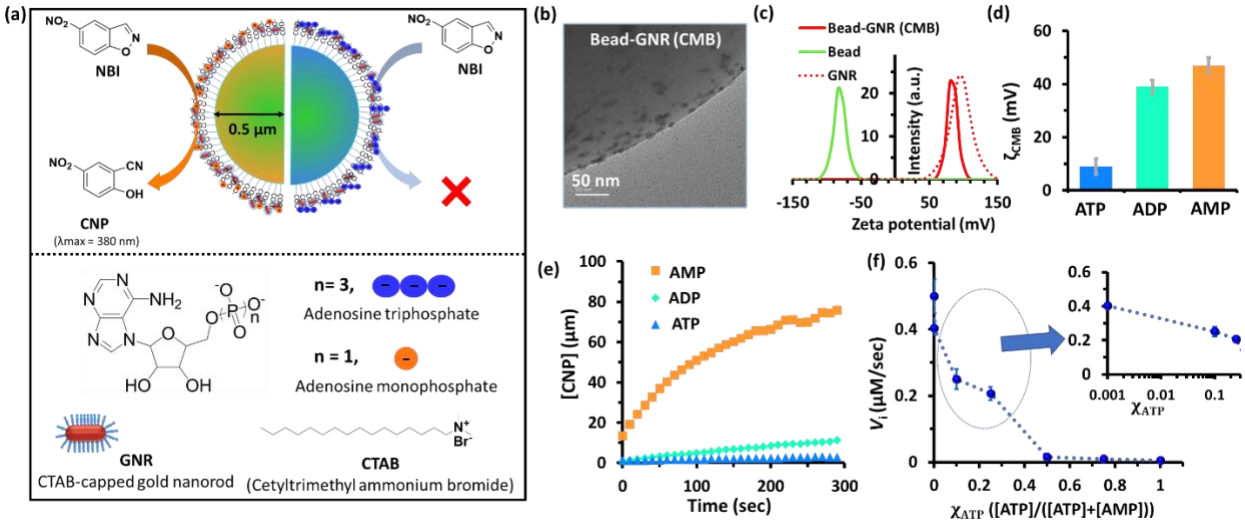

Figure 1. Characterization, nucleotide binding ability and reactivity of the colloid. (a) Schematic representation of a carboxylate-functionalized polystyrene bead modified with gold nanorods (CMB) catalyzing the Kemp elimination reaction, (b) TEM image of CMB conjugate showing GNR-bound bead surface. (c) Zeta potential profile of CMB, only beads, and GNR in water at 25 °C. (d) Zeta potential of CMB in the presence of adenosine-based nucleotides (1 mM). (e) Amount of Kemp elimination product (CNP) formed after addition of different nucleotides (1 mM) as a function of time. (f) Initial rate of CNP formation in presence of different fraction of ATP in a mixture of ATP and AMP.

Results and Discussions

Nucleotide binding ability and proton transfer reactivity of CMB

We synthesized catalytically active CMB as reported in the literature (details in supplementary information (SI)).[41] The carboxylate-functionalized polystyrene had a hydrodynamic diameter (D_h) of 1 μm and a zeta potential of -90 ± 5 mV. The overall zeta potential of the fluorescent CMB changed to +80 mV (nearly that of the GNR) upon conjugation with cationic GNR (length 23 ± 5 nm, width 6 ± 1 nm, and ζ = 100 ± 10 mV), indicating the binding and simultaneous reversal of the surface charge of the fluorescent CMB (Figure 1b-c, S1-S2, SI). We previously demonstrated the efficiency of this type of CMB in catalyzing the proton transfer reaction (also known as Kemp elimination (KE)) in the presence of phosphate buffer.[41,45] However, carboxylate beads devoid of nanoparticles exhibit no activity (Figure S9, SI). In another study, we demonstrated that the KE catalysis over a cationic gold nanoparticle surface can be controlled by modulating its multivalent interaction with AMP, ADP, and ATP.[45] Before quantifying how adenosine-based nucleotides would affect the CMB's propensity to catalyze KE, we first examined the binding ability of these nucleotides on the surface of the CMB. Expectedly, in the presence of nucleotides (at 1 mM concentration), the zeta potential of CMB (which is a measure of its surface charge) decreased to 47 ± 8, 39 ± 5 and 9 ± 4 mV with AMP, ADP, and ATP, respectively, indicating surface binding (Figure 1d, S3, SI). Across a range of concentrations between 0.01 and 10 mM of nucleotides, the difference in zeta potential of CMB in presence of ATP and AMP is highest at 1 mM concentration (Figure S4, SI). At 10 mM ATP, we observed lower stability of CMB as the zeta potential reaches only 3 ± 2 mV. Therefore, we used 1 mM concentration of nucleotides throughout, unless noted otherwise. Of all of the nucleotides, ATP binds most strongly due to the simultaneous interaction of three phosphate groups with GNR placed on the CMB surface.[13-14] Binding with ATP (1 mM) does not affect the stability of the CMB as no detachment of GNR from the bead was observed (Figure S6, SI).

Next, we measured the ability of the CMB to catalyze the KE reaction by following UV-scanning kinetics using 5-nitrobenzisoxazole (NBI) as a substrate and tracking the change of absorbance of the product (2-cyano nitrophenol (CNP)) peak at 380 nm (Figure S8, SI). In the absence of nucleotides, no catalysis was observed as the reaction followed the E2-pathway, which requires an anionic base (Figure S10, SI).[45-46] Interestingly, the reaction rate was enhanced significantly (almost 1000-fold) by the addition of 1 mM AMP to the system (Figure 1e). However,

the presence of a similar amount of ADP increased it only around 10-fold, and the addition of ATP did not improve catalysis. We also checked the catalysis in a mixed AMP/ATP system by changing the mole fraction of ATP from 0 to 1, while keeping the total concentration constant at 1 mM. (Figure 1f). We found that as ATP content increased, the KE catalytic ability decreased significantly (for instance in presence of 0.5 mM ATP and 0.5 mM AMP, almost no catalytic activity was observed. The pattern of catalytic activity in the presence of an AMP/ATP mixed nucleotide system was similar to our previously observed system with only cationic gold nanoparticles.[45] These findings suggest that the phenomenon of binding and nucleotide-mediated KE-catalysis modulation persists on the cationic surface of the GNR even when it is bound to an anionic micron-sized polymer bead.

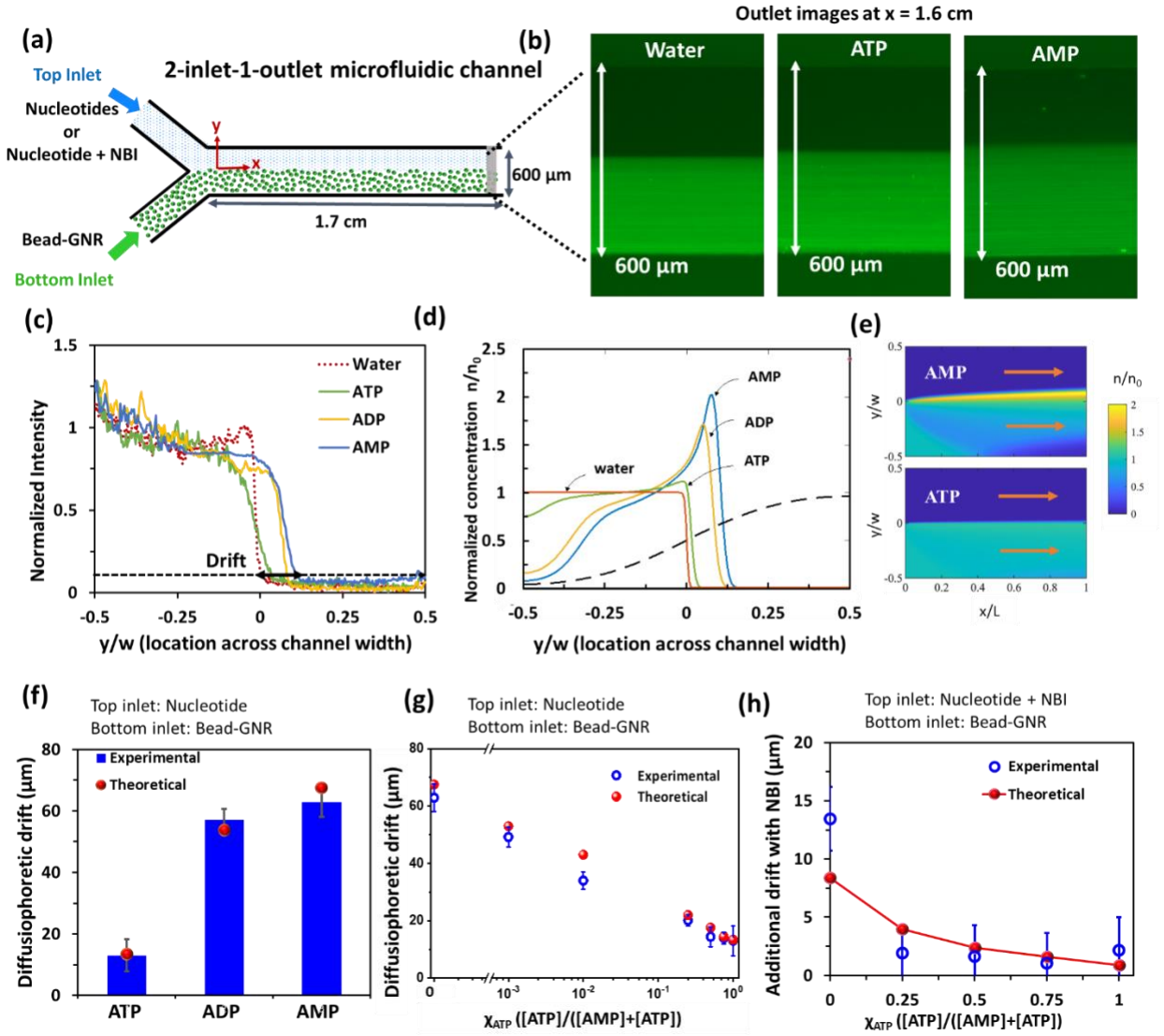

Figure 2. Diffusiophoretic drift of CMB in gradient of nucleotides under catalytic and non-catalytic conditions. (a) Schematic image showing the setup of the 2-inlet-1-outlet microfluidic experiment, where CMB has been passed through one inlet and nucleotides from the other and the fluorescence images were taken at the end of the channel at L =1.6 cm apart. Flow speed = 0.32 ml/h. (b) Representative image of the channel at the outlet showing accumulation of the fluorescent CMB towards AMP side is more than ATP and control. (c) Time-dependent fluorescence intensity profile at the outlet, from top to bottom end of the channel. The fluorescence is due to the presence of CMB (channel width = 600 µm). (d) Particle concentration profiles at the downstream end of the channel exposed to 1mM AMP, ADP and ATP obtained from the model. Concentrations are normalized in such a way that the integral across the channel width is conserved relative to the inlet. Particles drift due to diffusiophoresis towards higher concentrations of nucleotide (whose concentration is indicated as a dashed curve). The magnitude of drift follows

the ordering AMP>ADP>ATP, consistent with experiments. (e) Maps of particle concentration within the channel for AMP and ATP. The particle drift under exposure to ATP is negligible. (f) Experimental diffusiophoretic drift of CMB towards AMP, ADP and ATP when the concentration of nucleotides is 1 mM. Phoretic drift was calculated at a normalized intensity of 0.1 (near the baseline) as denoted by dotted line in Figure 2c. (g) Experimental diffusiophoretic drift of CMB towards gradient of nucleotides (AMP and ATP individually and in mixture) mixed with substrate, NBI (total concentration of nucleotides are 1 mM and NBI = 0.1 mM). χ_{ATP} is the mole fraction of ATP in a mixture of ATP and AMP i.e. [ATP]/([AMP]+[ATP]). In case of 2f and 2g, phoretic drift was calculated at a normalized intensity of 0.1 (near the baseline) as denoted by dotted line in Figure 2c. Error bar is the standard deviation of four independent sets of experiment. (h) Experimental and theoretical values of additional drift in presence of catalytic condition (i.e. in presence of nucleotides and NBI) compared to only nucleotides (only AMP or only ATP or mixture of AMP and ATP).

Experimental and theoretical investigation of diffusiophoretic drift of CMB in gradient of nucleotides

After establishing the charge neutralizing properties and the distribution of nucleotides around the cationic surface, we investigated how these multivalent binding interactions can modulate the diffusiophoresis of the CMB in a gradient of adenosine nucleotides. Diffusiophoretic phenomena consist of two main components – electrophoresis (motion due to a local electric field generated by a gradient of cations and anions with different diffusivities across the colloid) and chemiphoresis (motion driven by an osmotic pressure gradient across the particle).[28,34,35] Here, we studied the nucleotides' ability to produce phoretic drift in two different ways – (i) the individual phoretic effect of differently charged nucleotides and (ii) phoretic response in the presence of mixed nucleotides of different charges that compete to bind with the surface of the CMB.

For this purpose, we first used a microfluidic experiment with a two-inlet and one-outlet channel with dimensions of 17 × 0.6 × 0.1 mm^3 (length × width × height). We injected fluorescent CMB solution from one inlet and nucleotide (1 mM) from the other, each at a flow rate of $Q/2 =$ 0.16 ml/h, and observed the transverse drift of the CMB near the end of the channel (16 mm from the inlets merging) under a fluorescence microscope by scanning the zonal intensity (Figure 2a). The intensity was normalized with respect to its integral across the channel, which is a measure of the number of particles per area and is a conserved quantity at steady state. The diffusiophoretic drift due to the presence of nucleotides was calculated by comparing the location where the normalized intensity is 0.1 (near the baseline) with that of the no-nucleotide condition i.e., only in the presence of milli-Q water. Figure 2c shows the ratio of this drift to the channel width (width = 600 μm, constant across all experiments). Interestingly, we found that particles drift towards the nucleotide in the cases of AMP and ADP, with a drift of 63 ± 4 and 57 ± 3 μm, respectively. However, we observed no significant drift in presence of ATP gradient; the calculated drift was only 13 ± 5 μm (Figure 2b-d, S11-S14, Table S3, SI).

To understand the extent of drift in the experiments, we model the diffusiophoretic motion of particles in a co-flow geometry that mimics the experiment. We use a height averaged description of the fluid flow and the transport of nucleotides and particles (Figure 2e). Because the height of the channel $\boldsymbol{h}$ is much smaller than its width $\boldsymbol{w}$ in the experiments, the height-averaged velocity is approximately uniform across the channel and equals $u = Q/(wh)$.[47] At steady state, the height-averaged nucleotide concentration $c(x, y, t)$ is governed by the transport equation

$$\frac{\partial c}{\partial t} + u\frac{\partial c}{\partial x} = D\,\nabla^2 c, \tag{1}$$

where D is the ambipolar diffusivity of the nucleotides. The concentration of nucleotides follows a step distribution at the inlet to the channel.

Particles are transported by the flow and by diffusiophoresis due to gradients of the nucleotide, while also diffusing. The height-averaged concentration of particles, $n(x, y)$, is governed by

$$\frac{\partial n}{\partial t} + \nabla \cdot \left(\left(u\,\boldsymbol{e}_x + \boldsymbol{u}_{dp} \right) n \right) = D_p \nabla^2 n, \tag{2}$$

where $\boldsymbol{u}_{dp} = \Gamma_p\,\nabla\,(\ln\,c)$ is the diffusiophoretic velocity of a particle, Γ_p is its diffusiophoretic mobility, and D_p is its diffusivity. The particle concentration is also subject to zero flux at the walls ($\partial n/\partial y = 0$ at $y = \pm w/2$) and a step distribution of concentration at the inlet $n(x = 0, y, t) = n_0\,H(w/2 - y)$, with n_0 representing the particle concentration in the bottom inlet. We calculate the diffusiophoretic mobility Γ_p and the ambipolar diffusivity D by modeling the nucleotide in solution as a salt involving a mono- di- or tri-anion for AMP, ADP and AMP, respectively, with the appropriate number (one, two or three, respectively) of Na^+ cations.[26] We note that Γ_p depends on the zeta-potential of the particle (which we take directly from experimental measurements) and comprises a combination of an electrophoretic component and a chemiphoretic component; see SI.

We solve equations (1)–(2) numerically. The nucleotides diffuse across the channel producing concentration gradients that drive the phoretic motion of the particles. To compare with experiments, we report steady-state nucleotide and particle concentrations near the end of the channel ($L = 1.6$ mm from the inlet; cf. Figure 2). Figure 2(e) shows lateral profiles of normalized particle concentrations at the end of the channel. The normalization reflects the fact that the number of particles at any cross-section along the flow is constant. We find that the positively charged particles drift diffusiophoretically towards the nucleotide, consistent with the experiments. As seen in the experiments, AMP produces the greatest drift, followed by ADP, and then followed by ATP, which produces only a very weak drift. The extent of drift is controlled primarily by the differing

ζ-potential for these different nucleotides, with the differing ionic charge and diffusivities of the nucleotides playing a secondary role. We follow the experimental protocol and compute the drift as the location where the normalized concentration profiles attain a value of 0.1. The drift obtained with AMP is ~67.5 μm, which is in excellent agreement with the experimentally measured value of 66 ± 4 μm (Figure 2f). The agreement of the model with experiments is equally good with ADP and ATP. We remark that the model does not involve any fitting parameters, and all model parameters are extracted directly from experimental measurements (see SI for details). Theoretically, we also distinguished the contributions from chemiphoresis (motion driven by an osmotic pressure gradient across the particle) and electrophoresis (motion due to a local electric field generated by a gradient of cations and anions with different diffusivities across the colloid) to the particle motion in each case (Table S2, SI).

Many practical systems involve a mixture of nucleotides. Due to the drastic differences in different nucleotides' ability to drive phoretic drift, we investigated the phoretic drift in mixed nucleotide systems having different molar composition of AMP and ATP. In this case, it would be interesting to evaluate how much ATP is needed to resist the diffusiophoretic motion of CMB by AMP. We used a fraction of ATP, $\chi_{\mathrm{ATP}} = [\mathrm{ATP}]/([\mathrm{ATP}] + [\mathrm{AMP}])$ of 0, 0.01, 0.1, 0.25, 0.5, 0.75 and 1 (Figure S5, S15-19, Table S4, SI). Interestingly, we found that the drift started to decrease sharply after the addition of as little as 10 μM ATP (the solution also contains 990 μM of AMP; $\chi_{ATP} = 0.01$), and at $\chi_{\mathrm{ATP}} = 0.25$, the drift becomes almost negligible, decreasing from 66 μm to 14 μm. These observations clearly demonstrate that ATP-mediated interaction is effective on the cationic surface even at minute amounts; for example, 10% ATP fraction can suppress the AMP-mediated drift by 50%.

We also use the previously demonstrated modeling framework to understand the effect of a mixture of ATP and AMP. As before, we use the experimentally measured zeta potentials (cf. Figure S5, SI). Now, we track the transport of individual nucleotides and relate their concentration gradients to the diffusiophoretic particle velocity $\boldsymbol{u}_{dp}$ using a well-established theoretical framework for mixtures.[31,35] Similar to the experiments, the modeled drift drops rapidly in a mixture even with a small amount of ATP and decreases with increasing χ_{ATP}. As with single nucleotides, the theoretical prediction for the drift is in excellent quantitative agreement with experiments across all mixture compositions (Figure 2f).

In the recent literature, it has been shown that a catalyst (both enzyme or micro/nanoparticle based) migrates up the substrate gradient and the extent of migration depends on their catalytic activity and other conditions such as the presence or absence of a cofactor.[48-49] The extent and direction of drift is dominated by phoretic effects. This inspired us to explore the diffusiophoretic drift of the CMB in the microfluidic channel during proton transfer reactivity i.e. by adding substrate (NBI) with nucleotides as gradient. For this, we passed the substrate, NBI (1 mM) with nucleotide AMP (1 mM) or ATP (1 mM) or χ_{ATP} at 0.25 or 0.5 from one channel, and the beads through the other (Figure 2a). We then measured the drift of CMB near the end of the channel ($x = 1.6$ cm) under a fluorescent microscope. As already shown in Figure 1(f), the CMB showed KE catalysis only in the presence of large fractions of AMP, while the activity remained silent in both ATP and AMP + ATP (0.5 mM each) system. With added NBI also we expected to see additional shift of CMB towards the AMP+NBI side due to catalytic effects. With only AMP the drift was 63 ± 4 μm and with AMP+NBI it increased to 76 ± 3 μm (Figure 2g-h, S20-S26, Table S5). However, in non-catalytic conditions (ATP and AMP+ATP systems with NBI), little additional shift was observed. We hypothesize that the additional drift of the CMB is due to the slight increase of zeta potential of CMB while catalyzing the uncharged NBI on its surface (in the presence of AMP).[31-35] The calculated additional drift due to presence of NBI along with a mixture of AMP or ATP (over the case with only nucleotides without NBI) are close to experiments (Figure 2h). This lends credence to our hypothesis, suggesting that the effect of catalysis on the extent and direction of colloidal drift is controlled largely through its influence on the substrate polarity and therefore overall colloidal charge.

Phoretic drift of CMB in a macroscale system

Spatial cues at macroscopic scales are important in natural systems in the form of signaling gradients such as the extracellular matrix and for bone/cartilage development, and have also recently been applied in synthetic systems to understand reaction-diffusion kinetics and spatially segregated chemistry and morphogenesis.[50-54] We therefore investigated the ability of nucleotide gradients to drive diffusiophoretic motion in a macroscale system in absence of any continuous flow. Our macroscale experimental set up as shown in Figure 3a. Here, we added a 50 μl of either ATP or AMP or AMP + NBI through one arm and filled the chamber having dimension 40 × 10 × 0.05 mm^3 (length × width × height). The concentrations of nucleotides were maintained at 1 mM as in the microfluidic study. Next, we added 5 μl of the CMB (0.025 mg/ml bead, 5 times more

dilute than the concentration used in the microfluidic study) and followed the particle motion inside the chamber using the microscope. We followed the population dynamics at four zones, namely frame A, B, C, and D, each having length of 1.5 mm. We first performed a control experiment with only milli-Q water (without nucleotides or salts) and observed the motion behavior of CMB inside the chamber (Figure S27, SI), which is driven by particle diffusion, gravity and inertial effects. We then performed experiments in presence of nucleotides to isolate phoretic effects on the particle motion generated by nucleotide gradients. The CMB traveled farther in the presence of nucleotides (the motion is up the nucleotide gradient); see Figure 3. Furthermore, the drift was greater with AMP compared with ATP. Interestingly, using a combination of NBI and AMP was observed to result in a further 10% upgradient migration as compared with AMP alone (Figure 3, Figure S28-S29, SI). In all cases, we performed measurements up to 5 min as after that time, we observed settling of the particles at the bottom of the glass channel which is likely also due to interactivity of the cationic bead with the anionic glass surface (Figure S33, SI). Overall, we observed similar trends in phoretic drift in this macroscopic setup to the microfluidic experiments. Interestingly, we were able to generate almost 0.5 mm difference in the macroscopic case (almost one order of magnitude higher than microfluidic flow set up) in the diffusiophoretic drift of CMB when AMP was used instead of ATP (Figure 3b).

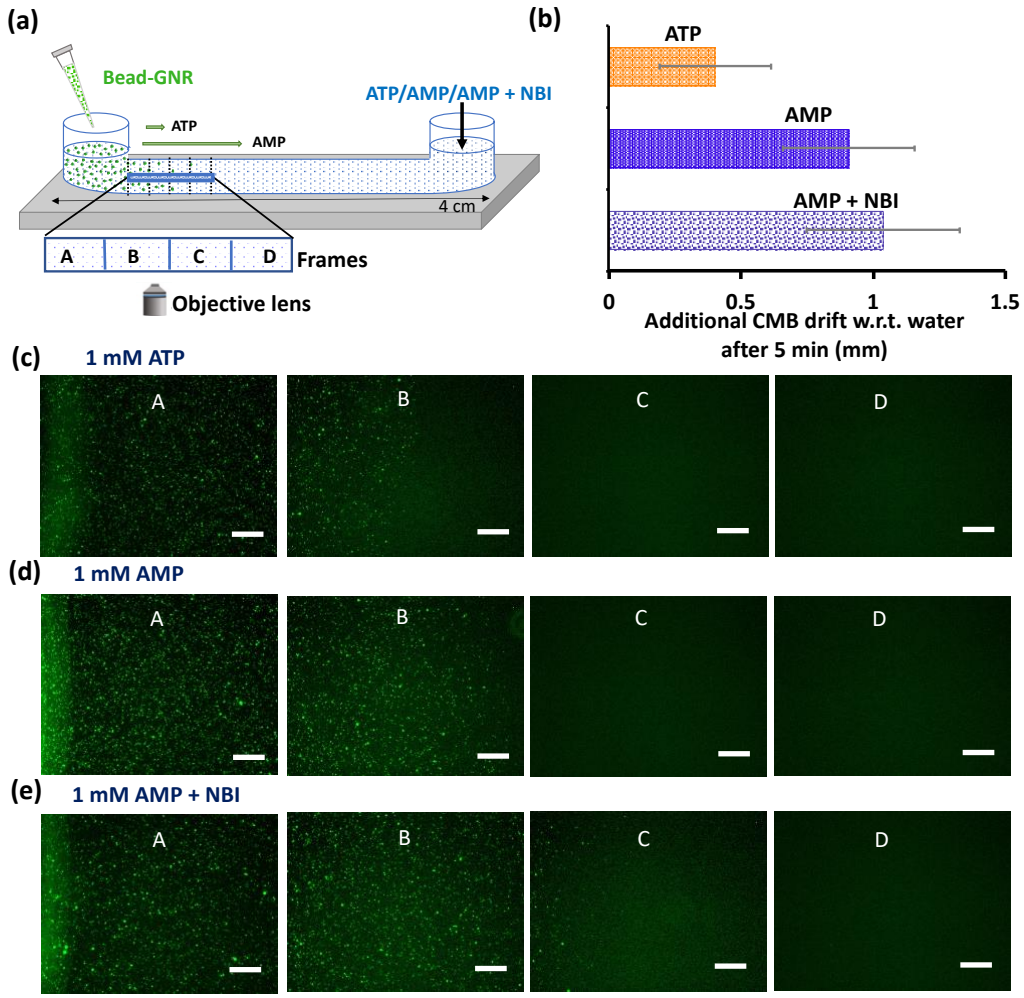

Figure 3. Macroscale manifestation of diffusiophoretic drift in gradient of nucleotides. (a) Schematic representation of the experimental set up. 50 µl of nucleotide solution with and without NBI solution was added from one end of channel and 5 µl CMB solution was added from another end. (b) Additional distance covered by CMB when channel was filled with ATP or AMP (1 mM) with and without NBI solution with respect to only water after 5 min. Fluorescence images of channel in different frames when (c) ATP, (d) AMP, (e) AMP + NBI solution was added. Scale bar of each image is 200 µm.

Phoretic leap of CMB during enzymatic ATP hydrolysis

We have already shown both experimentally and theoretically that multivalent interactions with ATP significantly modify diffusiophoretic motion in ATP/AMP mixtures (Figures 2f, g). We now exploit this feature to explore 'in situ' degradation of this multivalent interactivity, and its consequences for temporal modulation of phoresis and zone-specific population dynamics of the CMB. For in situ downregulation of multivalent interactivity, we chose potato apyrase enzyme

(PA), which cleaves ATP to AMP + 2 Pi. We note that this strategy has been used in recent literature to devise transient and dynamic self-assembled systems with applications including the design of programmed reactors and switchable catalysts.[20,55] However, how this effect can modulate complex non-equilibrium phoretic processes has not been previously explored. Uncovering this behavior across different length scales offers interesting advantages for modulating transport and spatiotemporal localization dynamics in diffusion-driven systems.

To this end, we used the macroscale set up as previously discussed (schematically shown in Figure 3a). In this case, we used only 10 μM ATP, as the complete hydrolysis of ATP occurs within 5 min at a PA concentration of 100 nM (see SI for enzyme kinetics, kcat, and Km values, Figure S35-S36, SI). At any time, the hydrolysis reaction produces a solution containing $10\ \chi_{\mathrm{ATP}}$ μM ATP + $10\ (1-\chi_{\mathrm{ATP}})$ μM AMP + $20\ (1-\chi_{\mathrm{ATP}})$ μM Pi, where the fraction of ATP $\chi_{\mathrm{ATP}} = [\mathrm{ATP}]/([\mathrm{ATP}]+[\mathrm{AMP}])$ decreases continually over time.

Before directly measuring the temporal dynamics of CMB due to ATP hydrolyzed by PA, we first performed steady-state control experiments (without enzyme) to mimic the chemical composition of the solution that would occur during this reaction. This makes the experimental follow-up of spatiotemporal dynamics in reaction conditions (i.e. with PA) more straightforward to understand. In our control experiments, we used compositions of ATP + AMP + Pi of the type described above (without PA) with ATP fractions χ_{ATP} = 0.1, 0.2, 0.4, 0.5, 0.7, and 0.9. As in earlier experiments with mixtures, we observed appreciable differences in ζ-potential of CMB with 10 μM ATP ($\chi_{ATP} = 1$; ζ = 30 ± 3 mV) versus 10 μM AMP + 20 μM Pi ($\chi_{ATP} = 1$; ζ = 50 ± 2 mV) (Figure S30, SI). The additional drift of CMB (with respect to milliQ water only) observed at χ_{ATP} values of 0 and 1 are 3 ± 0.5 and 1.2 ± 0.3 mm (Figure S31-S32, SI). Interestingly, this drift was observed to stay roughly constant upon decreasing χ_{ATP} value from 1 to 0.4, and a sudden increase in drift was observed when decreasing χ_{ATP} below 0.3 (Figure S33, SI). This experiment exemplifies the role of the multivalent binding in driving diffusiophoretic effects, as the number of phosphate units (covalently linked for ATP or free phosphate in case of AMP + 2Pi) is kept constant in all cases.

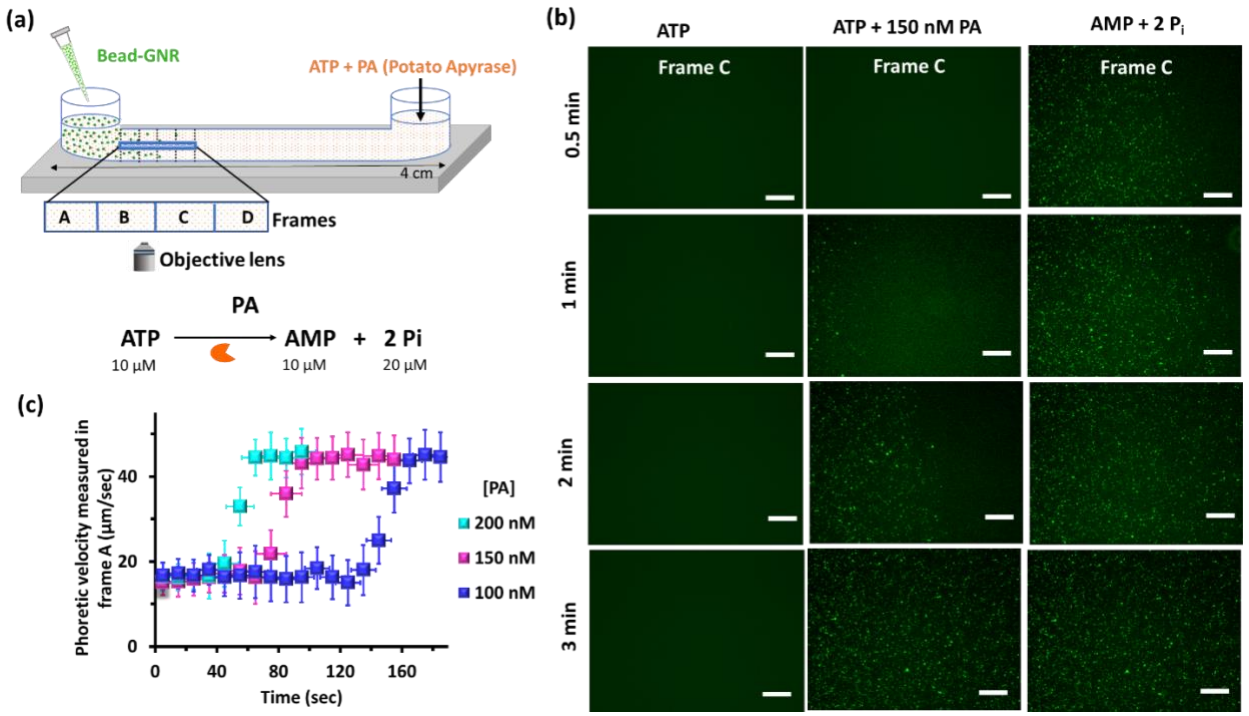

Figure 4. Spatiotemporal evolution of colloidal population dynamics during enzymatic hydrolysis of ATP. (a) Schematic representation of the experimental setup. ATP containing potato apyrase was filled inside channel and CMB solution was added from another end. (b) Temporal evolution of migration of CMB in frame C with time when ATP or AMP + 2Pi or ATP + PA (150 nM, ATP hydrolysis condition) was added inside channel. (c) Phoretic velocity of CMB measured in frame A during ATP hydrolysis at different PA concentration. The calculation was performed from the recorded video SV1 and SV2. Experimental condition: 0.025 mg/mL bead, [GNR] = 37.5 pM, [ATP] =10 µM, [PA] = 150 nM at 25 °C.

Next, we studied how this sensitivity of the phoresis to ATP fraction could be exploited to modulate the spatiotemporal dynamics of CMB by changing the valency of interaction in situ using the enzymatic hydrolysis of ATP. We filled the chamber with ATP (0.01 mM) and PA (100-200 nM) and then added CMB solution from one arm (Figure 4a). We then followed the particle population with time at frame C, as in the presence of ATP (without PA), no particle was present in that frame over the experimental time, whereas this frame was densely populated in the presence of AMP + 2Pi. With 150 nM PA, frame C started to become populated after only 1 min (Figure 4b). Using 100 or 200 nM PA instead led to a decrease or increase, respectively, of CMB particle density at frame C observed after 1 min (Figure S37, SI), confirming the role of ATP hydrolysis in controlling the motion of particles.

We also measured the diffusiophoretic velocity for the same experiment by tracking particle motion in frame A. In the presence of ATP but without PA, the drift velocity is around 15 ± 3 μm/s during our recording time of 3 min (Figure S38, SI). Interestingly, in presence of PA, the velocity was initially similar to the ATP-only case, and increases rapidly (i.e., "leaps") to over 40 μm/s after some time, where remained constant for the rest of the experiment. For example, in the presence of 200 nM PA, the drift velocity of CMB increased up to 45 μm/s from its initial velocity of 17 μm/s in a span of only 15 seconds (Figure 4c, SV1). We observed a similar trend for 150 nM and 100 nM of PA where the phoretic jump took almost 85, and 140 seconds to reach maximum velocity (Figure 4c, SV2). Our kinetic parameters suggest that the observed sudden leap in phoretic velocity occurs after dissociation of around 70% ATP. These observations demonstrated that - (i) phoretic leap of colloids is possible in a system by downregulating the multivalent interactivity with external counterparts. (ii) by tuning the drift velocity, the population density of colloid particles at a particular frame at different time intervals can also be modulated. In other words, spatiotemporal patterns can be altered simply by modulating the drift velocity of the colloids.

Conclusion

In summary, combining theoretical and experimental analysis, we explored how multivalent chemical fuel-driven interaction of catalytic microbeads with adenosine nucleotides modulate the diffusiophoretic drift of the bead in both microfluidic and millimeter-scale macroscopic environments. This study also illuminates the area of nucleotide-mediated catalytic processes and elucidates their effects on diffusiophoretic behavior and related spatiotemporal organization of particles.[56] Importantly, we demonstrated a new phenomenon, colloidal phoretic leap, that arises during in situ downregulation of multivalent interactivity. Additionally, the timing of the phoretic leap can be regulated by changing enzyme-mediated ATP hydrolysis, in this case. Here, only after around 70% degradation of ATP, results in sudden increase in colloidal phoresis. Overall, we showed a possible route of generating spatiotemporally controlled micron-sized colloidal patterns via fine tuning of multivalent interaction with small molecules. The main advantage of this technique is that delivery of colloid for either chemical processes, like catalysis or releasing drug/chemicals can be programmed both as a function of space and time as the drift velocity can

be switched on or off. The results of this research boost the creation of synthetic systems that emulate the defining properties of living matter by chemical gradient-sensing driven signaling systems in terms of their motility behavior.[57-62] Thus, it opens up opportunities for further research in multivalent interaction-mediated non-equilibrium chemistry induced by nucleotides, oligonucleotides, and DNA or RNA in driving the motion of colloidal particles and soft matter like liposomes of different shapes and sizes. These studies can have potential applications in designing synthetic spatiotemporally controlled catalytic systems to transport vehicle.

ASSOCIATED CONTENT

Supporting Information. Materials and methods, Synthesis of nanorods and CMB, Details of theoretical calculations, videos.

Notes

The authors declare no competing financial interest.

Acknowledgment

S.M. acknowledges financial support of Science and Engineering Research Board (SERB) (File No. SRG/2019/000365). E.S. acknowledges CSIR, India (09/947(0109)/2019-EMR-I) for doctoral research grant**.**

Abbreviations

KE, Kemp elimination reaction; NBI, 5-Nitrobenzisoxazole; CNP, 2-Cyanonitrophenol; GNR, Gold nanorods; CMB, carboxylic acid-modified polystyrene fluorescent bead electrostatically bound with a cationic cetyltrimethylammonium bromide (CTAB)-coated gold nanorod (GNR) on its surface.

References

1. Krishnamurthy, V. M.; Estroff, L. A.; Whitesides, G. M. *Multivalency in Ligand Design" in Fragment-Based Approaches in Drug Discovery*; Wiley-VCH: Weinheim, 2006.
2. Dernedde, J. *Multivalency in Biosystems*; John Wiley & Sons Ltd, 2017.
3. Fasting, C.; Schalley, C. A.; Weber, M.; Seitz, O.; Hecht, S.; Koksch, B.; Dernedde, J.; Graf, C.; Knapp, E.-W.; Haag, R. *Angew. Chem. Int. Ed* **2012**, *51*, 10472–10498.
4. Scheepers, M. R. W.; van IJzendoorn, L. J.; Prins, M. W. J. Multivalent Weak Interactions Enhance Selectivity of Interparticle Binding. *Proc. Natl. Acad. Sci. U. S. A.* **2020**, *117* (37), 22690–22697.
5. Kane, R. S. Thermodynamics of Multivalent Interactions: Influence of the Linker. *Langmuir* **2010**, *26* (11), 8636–8640.
6. Di Iorio, D.; Verheijden, M. L.; van der Vries, E.; Jonkheijm, P.; Huskens, J. Weak Multivalent Binding of Influenza Hemagglutinin Nanoparticles at a Sialoglycan-Functionalized Supported Lipid Bilayer. *ACS Nano* **2019**, *13* (3), 3413–3423.
7. Overeem, N. J.; van der Vries, E.; Huskens, J. A Dynamic, Supramolecular View on the Multivalent Interaction between Influenza Virus and Host Cell. *Small* **2021**, *17* (13), e2007214.
8. Zaramella, D.; Scrimin, P.; Prins, L. J. Self-Assembly of a Catalytic Multivalent Peptide-Nanoparticle Complex. *J. Am. Chem. Soc.* **2012**, *134* (20), 8396–8399.
9. Chan, C. W.; Smith, D. K. Pyrene-Based Heparin Sensors in Competitive Aqueous Media - the Role of Self-Assembled Multivalency (SAMul). *Chem. Commun.* **2016**, *52* (19), 3785–3788.
10. Bhatia, S.; Camacho, L. C.; Haag, R. Pathogen Inhibition by Multivalent Ligand Architectures. *J. Am. Chem. Soc.* **2016**, *138* (28), 8654–8666.
11. Zelikin, A. N.; Stellacci, F. Broad-Spectrum Antiviral Agents Based on Multivalent Inhibitors of Viral Infectivity. *Adv. Healthc. Mater.* **2021**, *10* (6), e2001433.
12. Lauster, D.; Glanz, M.; Bardua, M.; Ludwig, K.; Hellmund, M.; Hoffmann, U.; Hamann, A.; Böttcher, C.; Haag, R.; Hackenberger, C. P. R.; Herrmann, A. Multivalent Peptide-Nanoparticle Conjugates for Influenza-Virus Inhibition. *Angew. Chem. Int. Ed.* **2017**, *56* (21), 5931–5936.
13. Maiti, S.; Pezzato, C.; Garcia Martin, S.; Prins, L. J. Multivalent Interactions Regulate Signal Transduction in a Self-Assembled Hg2+ Sensor. *J. Am. Chem. Soc.* **2014**, *136* (32), 11288–11291.

14. Curk, T.; Dubacheva, G. V.; Brisson, A. R.; Richter, R. P. Controlling Superselectivity of Multivalent Interactions with Cofactors and Competitors. *J. Am. Chem. Soc.* **2022**, *144* (38), 17346–17350.
15. Zaupa, G.; Prins, L. J.; Scrimin, P. Resin-Supported Catalytic Dendrimers as Multivalent Artificial Metallonucleases. *Bioorg. Med. Chem. Lett.* **2009**, *19* (14), 3816–3820.
16. Badjić, J. D.; Nelson, A.; Cantrill, S. J.; Turnbull, W. B.; Stoddart, J. F. Multivalency and Cooperativity in Supramolecular Chemistry. *Acc. Chem. Res.* **2005**, *38* (9), 723–732.
17. Mulder, A.; Huskens, J.; Reinhoudt, D. N. Multivalency in Supramolecular Chemistry and Nanofabrication. *Org. Biomol. Chem.* **2004**, *2* (23), 3409–3424.
18. Kauscher, U.; Ravoo, B. J. Mannose-Decorated Cyclodextrin Vesicles: The Interplay of Multivalency and Surface Density in Lectin-Carbohydrate Recognition. *Beilstein J. Org. Chem.* **2012**, *8*, 1543–1551.
19. Shandilya, E.; Maiti, S. Deconvolution of Transient Species in a Multivalent Fuel-driven Multistep Assembly under Dissipative Conditions. *ChemSystemsChem* **2020**, *2* (2), e1900040.
20. Das, K.; Gabrielli, L.; Prins, L. J. Chemically Fueled Self-Assembly in Biology and Chemistry. *Angew. Chem. Int. Ed.* **2021**, *60* (37), 20120–20143.
21. Fialkowski, M.; Bishop, K. J. M.; Klajn, R.; Smoukov, S. K.; Campbell, C. J.; Grzybowski, B. A. Principles and Implementations of Dissipative (Dynamic) Self-Assembly. *J. Phys. Chem. B* **2006**, *110* (6), 2482–2496.
22. De, S.; Klajn, R. Dissipative Self-Assembly Driven by the Consumption of Chemical Fuels. *Adv. Mater.* **2018**, *30* (41), e1706750.
23. Corra, S.; Bakić, M. T.; Groppi, J.; Baroncini, M.; Silvi, S.; Penocchio, E.; Esposito, M.; Credi, A. Kinetic and Energetic Insights into the Dissipative Non-Equilibrium Operation of an Autonomous Light-Powered Supramolecular Pump. *Nat. Nanotechnol.* **2022**, *17* (7), 746–751.
24. Pezzato, C.; Cheng, C.; Stoddart, J. F.; Astumian, R. D. Mastering the Non-Equilibrium Assembly and Operation of Molecular Machines. *Chem. Soc. Rev.* **2017**, *46* (18), 5491–5507.
25. te Brinke, E.; Groen, J.; Herrmann, A.; Heus, H. A.; Rivas, G.; Spruijt, E.; Huck, W. T. S. Dissipative Adaptation in Driven Self-Assembly Leading to Self-Dividing Fibrils. *Nat. Nanotechnol.* **2018**, *13* (9), 849–855.
26. Wilson, J. L.; Shim, S.; Yu, Y. E.; Gupta, A.; Stone, H. A. Diffusiophoresis in Multivalent Electrolytes. *Langmuir* **2020**, *36* (25), 7014–7020.

27. Majhi, S.; Bhattacharyya, S. Numerical Study on Diffusiophoresis of a Hydrophobic Nanoparticle in a Monovalent or Multivalent Electrolyte. *Colloids Surf. A Physicochem. Eng. Asp.* **2022**, *648* (129272), 129272.
28. Derjaguin, B.; Sidorenkov, G.; Zubashchenkov, E.; Kiseleva, E. Kinetic Phenomena in Boundary Films of Liquids. *Kolloidn. Zh* **1947**, *9*, 335–347.
29. Prieve, D. C.; Anderson, J. L.; Ebel, J. P.; Lowell, M. E. Motion of a Particle Generated by Chemical Gradients. Part 2. Electrolytes. *J. Fluid Mech.* **1984**, *148* (1), 247–269.
30. Ebel, J. P.; Anderson, J. L.; Prieve, D. C. Diffusiophoresis of Latex Particles in Electrolyte Gradients. *Langmuir* **1988**, *4* (2), 396–406.
31. Gupta, A.; Rallabandi, B.; Stone, H. A. Diffusiophoretic and Diffusioosmotic Velocities for Mixtures of Valence-Asymmetric Electrolytes. *Phys. Rev. Fluids* **2019**, *4* (4).
32. Ault, J. T.; Warren, P. B.; Shin, S.; Stone, H. A. Diffusiophoresis in One-Dimensional Solute Gradients. *Soft Matter* **2017**, *13* (47), 9015–9023.
33. Nery-Azevedo, R.; Banerjee, A.; Squires, T. M. Diffusiophoresis in Ionic Surfactant Gradients. *Langmuir* **2017**, *33* (38), 9694–9702.
34. Shim, S. Diffusiophoresis, Diffusioosmosis, and Microfluidics: Surface-Flow-Driven Phenomena in the Presence of Flow. *Chem. Rev.* **2022**, *122* (7), 6986–7009.
35. Velegol, D.; Garg, A.; Guha, R.; Kar, A.; Kumar, M. Origins of Concentration Gradients for Diffusiophoresis. *Soft Matter* **2016**, *12* (21), 4686–4703.
36. Abécassis, B.; Cottin-Bizonne, C.; Ybert, C.; Ajdari, A.; Bocquet, L. Boosting Migration of Large Particles by Solute Contrasts. *Nat. Mater.* **2008**, *7* (10), 785–789.
37. Shin, S.; Shardt, O.; Warren, P. B.; Stone, H. A. Membraneless Water Filtration Using CO2. *Nat. Commun.* **2017**, *8* (1), 15181.
38. Prieve, D. C. Migration of a Colloidal Particle in a Gradient of Electrolyte Concentration. *Adv. Colloid Interface Sci.* **1982**, *16* (1), 321–335.
39. Staffeld, P. O. & Quinn, J. A. Diffusion-induced banding of colloid particles via diffusiophoresis. *J. Colloid Interface Sci.* **130**, 69–87 (1989).
40. Burkholder, E. W.; Brady, J. F. Tracer Diffusion in Active Suspensions. *Phys. Rev. E.* **2017**, *95* (5–1), 052605.
41. Shandilya, E.; Dasgupta, B.; Maiti, S. Interconnectivity between Surface Reactivity and Self-Assembly of Kemp Elimination Catalyzing Nanorods. *Chemistry* **2021**, *27* (29), 7831–7836.

42. Ramm, B.; Goychuk, A.; Khmelinskaia, A.; Blumhardt, P.; Eto, H.; Ganzinger, K. A.; Frey, E.; Schwille, P. A Diffusiophoretic Mechanism for ATP-Driven Transport without Motor Proteins. *Nat. Phys.* **2021**, *17* (7), 850–858.
43. Sear, R. P. Diffusiophoresis in Cells: A General Nonequilibrium, Nonmotor Mechanism for the Metabolism-Dependent Transport of Particles in Cells. *Phys. Rev. Lett.* **2019**, *122* (12), 128101.
44. Pizauro, J. M.; Ciancaglini, P.; Leone, F. A. Allosteric Modulation by ATP, Calcium and Magnesium Ions of Rat Osseous Plate Alkaline Phosphatase. *Biochim. Biophys. Acta* **1993**, *1202* (1), 22–28.
45. Mahato, R. R.; Shandilya, E.; Dasgupta, B.; Maiti, S. Dictating Catalytic Preference and Activity of a Nanoparticle by Modulating Its Multivalent Engagement. *ACS Catal.* **2021**, *11* (14), 8504–8509.
46. Priyanka; Shandilya, E.; Brar, S. K.; Mahato, R. R.; Maiti, S. Spatiotemporal Dynamics of Self-Assembled Structures in Enzymatically Induced Agonistic and Antagonistic Conditions. *Chem. Sci.* **2021**, *13* (1), 274–282.
47. Mortensen, N. A.; Okkels, F.; Bruus, H. Reexamination of Hagen-Poiseuille Flow: Shape Dependence of the Hydraulic Resistance in Microchannels. *Phys. Rev. E Stat. Nonlin. Soft Matter Phys.* **2005**, *71* (5).
48. Zhao, X. *et al.* Substrate-driven chemotactic assembly in an enzyme cascade. *Nat. Chem.* **10**, 311–317 (2018).
49. Agudo-Canalejo, J.; Illien, P.; Golestanian, R. Phoresis and Enhanced Diffusion Compete in Enzyme Chemotaxis. *Nano Lett.* **2018**, *18* (4), 2711–2717.
50. Aubert, S.; Bezagu, M.; Spivey, A. C.; Arseniyadis, S. Spatial and Temporal Control of Chemical Processes. *Nat. Rev. Chem.* **2019**, *3* (12), 706–722.
51. Chen, R.; Neri, S.; Prins, L. J. Enhanced Catalytic Activity under Non-Equilibrium Conditions. *Nat. Nanotechnol.* **2020**, *15* (10), 868–874.
52. Nguindjel, A.-D. C.; de Visser, P. J.; Winkens, M.; Korevaar, P. A. Spatial Programming of Self-Organizing Chemical Systems Using Sustained Physicochemical Gradients from Reaction, Diffusion and Hydrodynamics. *Phys. Chem. Chem. Phys.* **2022**, *24* (39), 23980–24001.
53. Shandilya, E.; Maiti, S. Self-Regulatory Micro- and Macroscale Patterning of ATP-Mediated Nanobioconjugate. *ACS Nano* **2023**, *17* (5), 5108–5120.

54. Bian, T.; Gardin, A.; Gemen, J.; Houben, L.; Perego, C.; Lee, B.; Elad, N.; Chu, Z.; Pavan, G. M.; Klajn, R. Electrostatic Co-Assembly of Nanoparticles with Oppositely Charged Small Molecules into Static and Dynamic Superstructures. *Nat. Chem.* **2021**, *13* (10), 940–949.
55. Dhiman, S.; Jain, A.; Kumar, M.; George, S. J. Adenosine-Phosphate-Fueled, Temporally Programmed Supramolecular Polymers with Multiple Transient States. *J. Am. Chem. Soc.* **2017**, *139* (46), 16568–16575.
56. Epstein, I. R.; Xu, B. Reaction-Diffusion Processes at the Nano- and Microscales. *Nat. Nanotechnol.* **2016**, *11* (4), 312–319.
57. Landge, A. N.; Jordan, B. M.; Diego, X.; Müller, P. Pattern Formation Mechanisms of Self-Organizing Reaction-Diffusion Systems. *Dev. Biol.* **2020**, *460* (1), 2–11.
58. Tian, L.; Li, M.; Liu, J.; Patil, A. J.; Drinkwater, B. W.; Mann, S. Nonequilibrium Spatiotemporal Sensing within Acoustically Patterned Two-Dimensional Protocell Arrays. *ACS Cent. Sci.* **2018**, *4* (11), 1551–1558.
59. Ragazzon, G.; Malferrari, M.; Arduini, A.; Secchi, A.; Rapino, S.; Silvi, S.; Credi, A. Autonomous Non-Equilibrium Self-Assembly and Molecular Movements Powered by Electrical Energy. *Angew. Chem. Int. Ed.* **2023**, *62* (5), e202214265.
60. Qiu, Y.; Feng, Y.; Guo, Q.-H.; Astumian, R. D.; Stoddart, J. F. Pumps through the Ages. *Chem* **2020**, *6* (8), 1952–1977.
61. Kathan, M.; Crespi, S.; Thiel, N. O.; Stares, D. L.; Morsa, D.; de Boer, J.; Pacella, G.; van den Enk, T.; Kobauri, P.; Portale, G.; Schalley, C. A.; Feringa, B. L. A Light-Fuelled Nanoratchet Shifts a Coupled Chemical Equilibrium. *Nat. Nanotechnol.* **2022**, *17* (2), 159–165.
62. Grzybowski, B. A. *Chemistry in Motion: Reaction-Diffusion Systems for Micro- and Nanotechnology*; Wiley-Blackwell: Hoboken, NJ, 2009.